AC Research

Anal. Chem. **2000,** *72,* 887−898

Accelerated Articles

Molecular Orientation and Angular Distribution Probed by Angle-Resolved Absorbance and Second Harmonic Generation

Garth J. Simpson, Sarah G. Westerbuhr, and Kathy L. Rowlen*

Department of Chemistry and Biochemistry, University of Colorado, Boulder, Colorado 80309-0215

Second harmonic generation (SHG) and angle-resolved absorbance with photoacoustic detection were combined to evaluate both the mean orientation angle and the width of the angular distribution for two surface-bound molecular systems. Assuming a Gaussian distribution function, a physisorbed stilbene dye on fused silica exhibited a narrow distribution centered at 73° with a root-mean-square (rms) width of less than ∼8°. In contrast, a covalently bound azo dye resulted in a broad orientation distribution (rms width of ∼30°) centered at 60°. It was also demonstrated that the combination of nonlinear (SHG) and linear (absorbance) spectroscopic techniques provides valuable insight into molecular orientation that a combination of two linear techniques (such as fluorescence and absorbance) is unable to provide.

The ability of monolayer and multilayer films to dramatically alter both the physical and optical properties of surfaces and interfaces has made them interesting systems to study for both fundamental and technological reasons.[1] Orientation measurements of surface-bound molecules provide valuable insight into the structure of thin films.[1,2] From a single spectroscopic orientation measurement, only a single parameter describing the orientation distribution can typically be generated. In some instances, fluorescence measurements alone can yield two orientation parameters, allowing for evaluation of the mean orientation angle and an approximation of the orientational distribution.[3−5] Saavedra and co-workers have employed a combination of absorbance and fluorescence in order to probe two orientation parameters for thin surface films.[6−10] In most spectroscopic studies, however, a narrow distribution is assumed and a single parameter is used to evaluate the apparent mean orientation angle. As demonstrated in refs 3−10, such an assumption is not always justified. Furthermore, even if the molecular system is highly oriented with respect to the local surface, surface roughness can broaden the orientation distribution sufficiently that the assumption of a narrow distribution may not be valid.[11−18]

A classic example of an instance in which the assumption of a narrow distribution may be misleading is that of absorbance measurements for molecular orientation angles equal to the magic angle of 54.7°, which is also the apparent orientation angle obtained from a random distribution. Absorbance measurements yielding an apparent orientation angle of 54.7° do not allow for distinction between the case in which every molecule is oriented in a narrow distribution centered at the magic angle and the case in which the molecules are randomly oriented. We have recently demonstrated that an equivalent magic angle exists for second harmonic generation orientation measurements.[19] Sufficiently

(1) Ulman, A. *An Introduction to Ultrathin Organic Films: From Langmuir−Blodgett to Self-Assembly*; Academic Press: New York, 1991.
(2) Ulman, A., Ed. *Characterization of Organic Thin Films*; Butterworth-Heinemann: Boston, 1995.
(3) Bos, J. A.; Kleijn, J. M. *Biophys. J.* **1995**, *68*, 2573−2579.
(4) Yang, J.; Kleijn, J. M. *Biophys. J.* **1999**, *76*, 323−332.
(5) Zhia, X.; Kleijn, J. M. *Biophys. J.* **1997**, *72*, 2651−2659.
(6) Edmiston, P. L.; Lee, J. E.; Cheng, S.-S.; Saavedra, S. S. *J. Am. Chem. Soc.* **1997**, *119*, 560−570.
(7) Wood, L. L.; Cheng, S.-S.; Edmiston, P. L.; Saavedra, S. S. *J. Am. Chem. Soc.* **1997**, *119*, 561−576.
(8) Edmiston, P. L.; Saavedra, S. S. *Biophys. J.* **1998**, *74*, 999−1006.
(9) Edmiston, P. L.; Saavedra, S. S. *J. Am. Chem. Soc.* **1998**, *120*, 1665−1671.
(10) Edmiston, P. L.; Lee, J. L.; Wood, L. L.; Saavedra, S. S. *J. Phys. Chem.* **1996**, *100*, 775−784.
(11) Piasecki, D. A.; Wirth, M. J. *Langmuir* **1994**, *10*, 1913−1918.
(12) Piasecki, D. A.; Wirth, M. J. *J. Phys. Chem.* **1993**, *97*, 7700−7705.
(13) Wirth, M. J.; Burbage, J. D. *J. Phys. Chem.* **1992**, *96*, 9022−9025.
(14) Burbage, J. D.; Wirth, M. J. *J. Phys. Chem.* **1992**, *96*, 5943−5948.
(15) Simpson, G. J.; Rowlen, K. L. *J. Phys. Chem. B* **1999**, *103*, 1525−1531.
(16) Simpson, G. J.; Rowlen, K. L. *J. Phys. Chem. B* **1999**, *103*, 3800−3811.
(17) Simpson, G. J.; Rowlen, K. L. *Chem. Phys. Lett.* **1999**, *309*, 117−122.
(18) Simpson, G. J.; Rowlen, K. L. *Chem. Phys. Lett.*, in press.
(19) Simpson, G. J.; Rowlen, K. L. *J. Am. Chem. Soc.* **1999**, *121*, 2635−2636.

10.1021/ac9912956 CCC: $19.00
Published on Web 02/01/2000

broad orientation distributions probed by second harmonic generation (SHG) will yield apparent orientation angles of 39.2°, regardless of the true distribution mean. Analogous to the magic angle for absorbance, if a single SHG measurement yields the SHG magic angle result, it is impossible to determine whether the measurement represents a narrow distribution centered around 39.2° or a broad distribution.

It is evident that the width of an orientation distribution can be as important as the mean orientation angle. Methods that allow for investigation of both the distribution mean and width about that mean provide a more complete and intuitive description of molecular orientation.[3−10] In this report, an absorbance technique (angle-resolved absorbance by photoacoustic detection, or ARAPD) is combined with SHG to evaluate the mean molecular orientation angle and the angular distribution about the mean for two distinct molecular systems. In the following sections, a complete description of the necessary mathematical relationships for ARAPD and SHG orientation measurements is presented.

Angle-Resolved Absorbance. ARAPD is a technique developed in our laboratory for submonolayer to multilayer absorbance orientation measurements at dielectric surfaces.[20,21] ARAPD measurements rely on the inherent sensitivity of photoacoustic detection to allow for minimal-background absorbance measurements with submonolayer detection limits.[20] For a moderately intense, unfocused pulsed laser beam, as used in these experiments, the photoacoustic signal generated arises solely from heat deposition, and not from high-intensity effects such as electrostriction or ablation. Consequently, a model describing the observed photoacoustic response of an optically thin sample at the interface may be formulated by minor modifications of a simple model previously presented by Tam et al.[22,23] For a photoacoustic wave generated from an optically thin sample at the interface between two media (1 and 2) of different thermal and acoustic properties, the photoacoustic amplitude generated in medium 1 is given by

$$S_{\mathrm{PAS},1} \propto (E_0\theta\sigma_{\mathrm{abs}})\,\frac{\beta_1}{\rho_1(c_1\rho_1C_{\mathrm{p}1} + c_2\rho_2C_{\mathrm{p}2})} \qquad (1)$$

in which $S_{\mathrm{PAS},1}$ is the photoacoustic amplitude within medium 1 some distance from the interface, E_0 is the incident energy of the excitation beam (mJ/pulse), θ is the surface coverage (molecules/cm^2), σ_{abs} is the absorption cross section of the surface dye molecules (cm^2/molecule), and β_i, ρ_i, and C_{pi} are the thermal expansion coefficient, density, and heat capacity at constant pressure for medium i, respectively. The derivation of eq 1 from the original one-medium model by Tam et al. is provided in Appendix I. For the purposes of this study, the most important aspect of eq 1 is that the photoacoustic amplitude is directly proportional the absorption cross section, σ_{abs}, which itself is a function of the molecular orientation and the orientation of the incident electric field polarization.

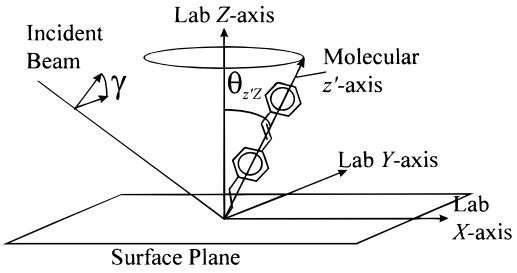

Figure 1. Definitions of relevant axes and angles. The molecular orientation angle, $\theta_{z'Z}$ is the angle between the molecular long axis (z') and the surface normal (lab Z-axis). The polarization rotation angle of the incident beam, γ, is defined such that $\gamma = 0°$ is p-polarized and $\gamma = 90°$ is s-polarized.

By varying the orientation of the electric field polarization vector with respect to the surface and tracking the resulting trend in absorbance (and correspondingly in photoacoustic amplitude), the ensemble-averaged orientation of a particular transition moment may be determined and from that the molecular orientation within the surface film. Mathematically, this measurement is described by the following expression:[24]

$$A_{\mathrm{tot}} = \langle(\mathbf{E}\cdot\mathbf{f})^2\rangle = |\mathbf{f}|^2|\mathbf{E}|^2[|e_X|^2K_{fX} + |e_Y|^2K_{\mathrm{f}Y} + |e_Z|^2K_{\mathrm{f}Z}] \qquad (2)$$

where A_{tot} is the sample absorbance, $\mathbf{E}$ is the incident electric

$$K_{fi} \equiv \langle\cos^2\theta_{fi}\rangle \qquad (3)$$

field polarization vector with components at the interface per unit incident amplitude of e_X, e_Y, and e_Z, $\mathbf{f}$ is the transition moment vector, and θ_{fi} is the angle between the transition moment vector and the laboratory i-axis, with the Z-axis directed normal to the surface. Since expectation values of squared cosines appear frequently in discussions of angle-resolved absorbance, they are abbreviated by the letter K, with subscripts indicating the corresponding angle.

If it is assumed for the moment that the probed transition moment lies parallel to the long molecular axis (the z'-axis, as shown in Figure 1) of a rodlike molecule, then $K_{\mathrm{f}Z}$ may be replaced by $K_{z'Z}$. The orientation parameter $K_{z'Z}$ is experimentally determined from absorbance measurements, and describes the polar angle between the molecular orientation axis (z') and the surface normal (Z). For different internal transition moment orientations (i.e., not parallel with the long molecular axis), analogous relations between $K_{\mathrm{f}Z}$ and the orientation angles of the molecular axes have been previously derived.[16,24] Combining the law of cosines (which states that $K_{z'X} + K_{z'Y} + K_{z'Z} = 1$) with the relation $K_{z'X} = K_{z'Y}$ (true for a random distribution within the surface plane), the absorbance expression in eq 2 can be rewritten:

$$A_{\mathrm{tot}} \propto |e_X|^2 + |e_Y|^2 + K_{z'Z}(2|e_Z|^2 - |e_X|^2 - |e_Y|^2) \qquad (4)$$

The electric field components at the interface are generated by

(20) Doughty, S. K.; Rowlen, K. L. *J. Phys. Chem.* **1995**, *99*, 2143−2150.
(21) Doughty, S. K.; Simpson, G. J.; Rowlen, K. L. *J. Am. Chem. Soc.* **1998**, *120*, 7997−7998.
(22) Hutchins, D. A.; Tam, A. C. *IEEE Trans. Ultrason., Ferroelectr., Freq. Control* **1986**. *UFFC-33*, 429−449.
(23) Patel, C. K. N.; Tam, A. C. *Rev. Mod. Phys.* **1981**, *53*, 517−550.
(24) Michl, J.; Thulstrup, E. K. *Spectroscopy with Polarized Light: Solute Alignment by Photoselection, in Liquid Crystals, Polymers, and Membranes*; VCH Publishers Inc.: New York, 1995; Chapter 5.

projection of the incident electric field onto the surface coordinate system, with Fresnel correction factors accounting for reflection and refraction at the interface:

$$|e_X|^2 = |\cos\vartheta_I \cos\gamma L^{\omega}_{XX}|^2 \quad (5a)$$

$$|e_Y|^2 = |\sin\gamma L^{\omega}_{YY}|^2 \quad (5b)$$

$$|e_Z|^2 = |\sin\vartheta_I \cos\gamma L^{\omega}_{ZZ}|^2 \quad (5c)$$

where ϑ_I is the angle of incidence with respect to the surface normal, γ is the polarization rotation angle ($\gamma = 0°$ for *p*-polarized light, $\gamma = \pm 90°$ for *s*-polarized light), and L^{ω}_{ii} are Fresnel factors that describe the electric field components at the interface per unit field directed along the *i*-axis. Explicit expressions for the Fresnel factors are presented in Appendix III for the total internal reflection cell used in these investigations.

As can be seen in eq 5, there are two simple approaches for altering the electric field at the interface: (1) vary the angle of incidence for *p*-polarized light ($\gamma = 0°$), or (2) rotate the plane of polarization for a fixed angle of incidence. For the latter approach with a constant angle of incidence, eq 4 can be rewritten:

$$A_{tot} \propto a_X \cos^2\gamma + a_Y \sin^2\gamma + K_{z'Z}(2a_Z \cos^2\gamma - a_X \cos^2\gamma - a_Y \sin^2\gamma) \quad (6a)$$

or

$$A_{tot} \propto a_X + (a_Y - a_X)\sin^2\gamma + K_{z'Z}[\sin^2\gamma(2a_Z - a_X + a_Y) + a_X - 2a_Z] \quad (6b)$$

where the factors a_i describe the electric field intensities of each component at the interface neglecting the dependence on the polarization rotation angle (e.g., $a_X = |\cos\vartheta_I L^{\omega}_{XX}|^2$). Since the fitting coefficients, a_i, are all known constants for a particular system and geometry, a fit of absorbance as a function of polarization rotation angle yields the value of the orientation parameter, $K_{z'Z}$. The experimentally determined orientation parameter is, in turn, related to the molecular orientation angle, $\theta_{z'Z}$, by an ensemble average of $\cos^2\theta_{z'Z}$:

$$K_{z'Z} = \langle\cos^2\theta_{z'Z}\rangle = N\int_0^{\pi}\cos^2\theta_{z'Z}\,P(\theta_{z'Z})\sin\theta_{z'Z}d\theta_{z'Z} \quad (7)$$

where $P(\theta_{z'Z})$ is the distribution function for $\theta_{z'Z}$ and N is a normalization constant. If the orientation distribution is sufficiently narrow, such that a δ-function may be assumed for $P(\theta_{z'Z})$, the mean orientation angle may be approximated as follows:

$$K_{z'Z} = \langle\cos^2\theta_{z'Z}\rangle \approx \cos^2\langle\theta_{z'Z}\rangle \quad (8)$$

where $\langle\theta_{z'Z}\rangle$ is the apparent molecular orientation angle, calculated if a narrow orientation distribution is assumed.

Second Harmonic Generation. SHG is the frequency doubling of light and, within the electric dipole approximation for light, is symmetry forbidden in random media but allowed for molecules oriented at the interface between two such media. Molecular orientation may be evaluated from measurements of the intensity and polarization of the second harmonic light generated under various polarization conditions of the fundamental beam. Interpretation of the experimental data is simplified considerably if only one molecular hyperpolarizability tensor element is dominant (which is often the case) and both the fundamental and second harmonic frequencies are far from a molecular resonance (such that Kleinman symmetry may be assumed[25]).

The intensity of the second harmonic light generated at an interface, $I^{2\omega}$, is given by the following relation:[26]

$$I^{2\omega} = \frac{32\pi^3\omega^2\sec^2\vartheta^{2\omega}}{c^3}|\mathbf{e}^{2\omega}\cdot\chi^{(2)}:\mathbf{e}^{\omega}\mathbf{e}^{\omega}|^2(I^{\omega})^2 \quad (9)$$

in which the superscripts ω and 2ω indicate parameters evaluated for either the fundamental frequency or the second harmonic, respectively, $\vartheta^{2\omega}$ is the angle between the surface normal and the propagation direction of the second harmonic, c is the speed of light, ω is the angular frequency of light, $\mathbf{e}^{\omega}$ is a vector describing the fundamental electric field amplitude at the interface, $\mathbf{e}^{2\omega}$ describes the polarization state of the second harmonic, and $\chi^{(2)}$ is the third-ranked, second-order nonlinear polarizability tensor. For SHG measurements with a molecular orientation distribution that is isotropic within the surface plane (consistent with most experiments), there are only three nonzero independent tensor elements: χ_{ZZZ}, χ_{ZXX}, and χ_{XXZ}.[26−28]

The *s*- and *p*-polarized components of the second harmonic intensity are typically measured independently, with the relationship between the measured intensities and the three independent tensor elements given by the following expressions:[26,28]

$$I_s = C|s_1\sin2\gamma^{\omega}\chi_{XXZ}|^2(I^{\omega})^2 \quad (10)$$

$$I_p = C|s_5\chi_{ZXX} + \cos^2\gamma^{\omega}(s_2\chi_{XXZ} + s_3\chi_{ZXX} + s_4\chi_{ZZZ} - s_5\chi_{ZXX})|^2(I^{\omega})^2 \quad (11)$$

where I_s and I_p are the measured *s*- and *p*-polarized second harmonic intensities, respectively, and the s_i are fitting coefficients that depend on both the fundamental and second harmonic electric fields at the interface. Details of the fitting procedure used are described in Appendix II. Explicit expressions for the fitting coefficients for SHG measurements in the total internal reflection geometry of this study are provided in Appendix III, including both the linear and nonlinear Fresnel correction factors for reflection and refraction.

Once relative values of the surface hyperpolarizability tensor elements have been obtained from fits of the experimental data to eqs 10 and 11, the SHG orientation parameter, $D_{z'Z}$, may be evaluated. For rodlike molecules, $D_{z'Z}$ is given by[27,29]

(25) Kleinman, D. A. *Phys. Rev.* **1962**, *126*, 1977−1979.
(26) Corn, R. M.; Higgins, D. A. *Chem. Rev.* **1994**, *94*, 107−125.
(27) Heinz, T. F. *Nonlinear Surface Electromagnetic Phenomena*; North-Holland: New York, 1991; pp 354−416.
(28) Dick, B.; Gierulski, A.; Marowsky, G.; Reider, G. A. *Appl. Phys. B* **1985**, *38*, 107−116.
(29) Dick, B. *Chem. Phys.* **1985**, *96*, 199−215.

$$D_{z'Z} \equiv \frac{\langle \cos^3 \theta_{z'Z} \rangle}{\langle \cos \theta_{z'Z} \rangle} = \frac{\chi_{ZZZ}}{\chi_{ZZZ} + 2\chi_{ZXX}} \qquad (12)$$

Analogous to the absorbance orientation parameter, $K_{z'Z}$, the SHG orientation parameter depends on the angle between the molecular long axis (z') and the surface normal (Z) through averages of cosine functions. Furthermore, for narrow molecular orientation distributions in which a δ-function probability distribution is reasonably accurate, the orientation parameters measured by SHG and ARAPD ($D_{z'Z}$ and $K_{z'Z}$, respectively) should be identical.

$$K_{z'Z} \approx D_{z'Z} \approx \cos^2\langle \theta_{z'Z} \rangle \qquad (13)$$

In cases for which the orientation distribution is not well-represented by a δ-function, the two orientation parameters may be significantly different. Combining SHG and ARAPD measurements of the same system under the same conditions allows for a convenient test of the narrow distribution assumption: if the distribution is sufficiently narrow, both measurements will yield identical results for the two orientation parameters, if not, both the mean and width of the distribution may be determined.

EXPERIMENTAL SECTION

ARAPD experiments were conducted using the third harmonic (355 nm) of a Q-switched Nd:YAG laser (Spectra Physics GCR-11). After separation of the third harmonic using appropriate dichroic mirrors, the 355 nm beam was passed through a quartz window, an aperature, a Glan laser prism, a stepper motor-controlled half-wave plate, and the total internal reflection cell (see Figure 2a). A portion of the 355 nm beam reflected off the quartz window was directed toward a photodoide to record the beam intensity during data acquisition. The total internal reflection flow cell (shown in Figure 2c) consisted of 50 μm thick Teflon spacer (Dupont FEP, 200CLZ) sandwiched between a fused-silica prism (Melles-Griot or Esco, S1-UV) and a UV-grade fused-silica microscope slide (Esco). Two holes in the microscope slide allow for the flow of solvent through the cell for acoustic coupling. A piezoelectric transducer (Panametrics) was coupled to the microscope slide and spatially offset from the spot of total internal reflection to temporally separate the photoacoustic wave from artifacts due to scattered light. After signal amplification, the acoustic waveforms were signal averaged on an oscilloscope, and the amplitude was transferred to a personal computer as a function of the excitation beam polarization rotation angle.

SHG data were acquired using the same flow cell as for the ARAPD investigations. The Nd:YAG fundamental (1064 nm) was passed through a visible-blocking filter, a quartz window, an aperature, a Glan laser prism, a stepper motor-controlled half-wave plate, a focusing lens, and the TIR flow cell. After the flow cell, the second harmonic beam was directed through an IR-blocking filter, a dichroic sheet polarizer, and a 532 nm interference filter and finally to a photomultiplier tube (PMT), shown in Figure 2b. The signal-averaged PMT response was recorded on an oscilloscope and the amplitude transferred to a personal computer as a function of the fundamental beam polarization rotation angle for both *s*- and *p*-polarized second harmonic

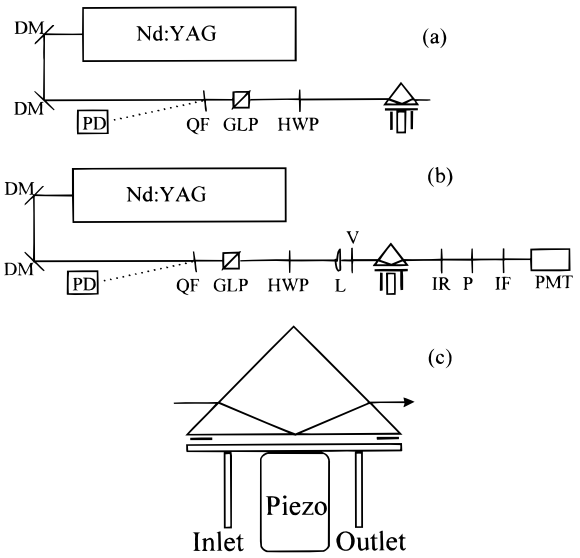

Figure 2. Experimental apparatus. (a) Schematic of the ARAPD apparatus: DM, dichroic mirror; PD, photodiode; QF, quartz flat; GLP, Glan laser prism; HWP, half-wave plate; (b) Schematic of the SHG apparatus: V, visible blocking filter; L, lens (20 cm focal length); IR, infrared blocking filter; P, polarizer (dichroic sheet); IF, 532 nm interference filter; PMT, photomultiplier tube. (c) Blowup of the total internal reflection flow cell. The cell consists of a 50 μm thick Teflon spacer sandwiched between a quartz prism and a quartz microscope slide. The piezoelectric transducer attached to the quartz slide is acoustically coupled to the prism by the solvent in the flow cell.

intensities. As with the ARAPD measurements, the incident beam intensity was recorded in conjunction with the signal intensity by reflecting a portion of the fundamental off a quartz window onto a photodiode. All reported SHG data have been normalized for the fundamental intensity.

Surface films of 1-docosyl-4-(4-hydroxystyrl)pyridinium bromide (DPB, Aldrich) were prepared by dipping a substrate into a chloroform (Fisher, Optima grade) solution of the dye. Prior to film formation, substrates were cleaned by sequential sonication in acetone, chloroform, and methanol, followed by drying under nitrogen. The substrates were further cleaned and hydroxylated by subsequent immersion for 5 min in a freshly prepared hot "piranha" solution (three parts 30% hydrogen peroxide, seven parts concentrated sulfuric acid, heated until oxygen bubbles freely form), followed by thorough rinsing in 18.2 MΩ filtered water, and drying under nitrogen. The substrates were then immersed in the dye solutions for 3 min prior to slow removal (no dependence of the film thickness on dip time was observed). Ellipsometric thicknesses (AutoEL ellipsometer, Rudolph Research) of the DPB films were acquired on dipped silicon wafers, assuming a monolayer refractive index of 1.5 (appropriate for a primarily aliphatic monolayer[1]). DPB monolayer films for the ARAPD and SHG investigations were prepared directly on the TIR prism surface, with dye removed from the non total internal reflection (non-TIR) surfaces by wiping with a methanol-soaked Kimwipe. Monolayer formation was confirmed both by the ellipsometric thickness measurements and by UV−visible spectra of dipped quartz flats, indicating the presence of the dye (acquired with a Hewlett-Packard 8452A diode array spectrometer). The DPB monolayer films were analyzed in contact with pure hexanes (Fisher, Optima grade) and saturated DPB in hexanes in the flow

cell. A small signal loss was observed during data acquisition using pure hexanes, probably due to either photochemical effects or surface desorption, but no change in orientation resulted.

Monolayers of 4-(dimethylamino)azobenzene were covalently bound to the fused-silica total internal reflection prisms (Melles Griot or Esco, S1-UV). Prior to derivatization, the substrates were cleaned and hydroxylated using the same procedure as for the DPB substrates. For the first reaction step, the substrates were refluxed for 2 h in a solution of dry toluene (certified ACS, Fisher Scientific), 0.05 M pyridine (certified ACS, Fisher Scientific) and 0.02 M (3-aminopropyl)dimethylethoxysilane (Gelest). The substrates were then rinsed in toluene, sonicated in acetone, chloroform, and methanol, and dried under a flow of nitrogen. For the second reaction step, the substrates were placed in a solution of dry toluene, 0.075 M *N*,*N*-diisopropylethylamine (99.5%, Aldrich), and 0.8 mM 4-(dimethylamino)azobenzene-4′-sulfonyl chloride (Fluka Chemie) at room temperature with stirring overnight. Following the reaction, the substrates were rinsed in toluene and chloroform, sonicated in acetone, chloroform, and methanol, and dried under a flow of nitrogen. To prepare the azo dye in solution, the same reaction procedure was used except the dye was reacted with a 0.030 M propylamine (99+%, Aldrich) solution in toluene rather than the aminated surface. Water contact angles were measured before and after surface reaction on a home-built rotating stage with droplet images acquired by an optical microscope coupled to a CCD digitizing camera. Ellipsometric thickness measurements and UV−visible measurements were made using the same instruments as previously described. The organic layer was removed from the non-TIR faces of the prisms by dropping hot pirahna solution onto the horizontally positioned surfaces and allowing the pirahna to react for 15 min, followed by thorough rinsing with water and drying under a flow of nitrogen.

Molecular modeling calculations for both DPB and the azo dye were performed using Hyperchem (Hypercube, release 4) with geometry optimization performed using the AM1 semiempirical method, and electronic structure calculations performed with the ZINDO/S method.

RESULTS AND DISCUSSION

To extract meaningful orientation information using a TIR geometry, the influence of reflection and refraction at both the entrance and exit prism surfaces, as well as the amplitudes of the electric field components at the total internal reflection interface, must be known and accurate. Theoretical curves for the expected angle-resolved photoacoustic response for several different molecular orientations accounting for these effects are shown in Figure 3. The curves were generated using eq 6 with the Fresnel factors and fitting coefficients described in Appendix III. For surface-bound molecules with small orientation angles (aligned nearly parallel with the surface normal), the maximum photoacoustic amplitude is expected for *p*-polarized excitation ($\gamma = 0°$) with a minimum for *s*-polarized excitation. For molecules with large orientation angles (aligned nearly parallel with the surface plane), the exact opposite trend is observed.

For a polarization rotation angle near 55°, all molecular orientations yield the same photoacoustic response. This polarization angle is the equivalent of the absorbance magic angle after correcting for reflection, refraction, and total internal reflection surface fields. The polarization rotation angle yielding orientation-independent absorbance, γ^*, will be the value of γ for which the coefficient of $K_{z'Z}$ in eq 6 is equal to zero.

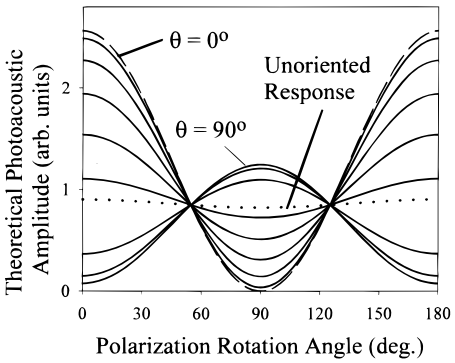

Figure 3. Theoretical ARAPD response curves accounting for reflection and refraction, including both real and imaginary contributions to the electric fields at the total internal reflection interface. The dashed line indicates the theoretical response for a molecular orientation normal to the surface, with each solid curve corresponding to a 10° increment in orientation angle. The dotted curve is the response expected from an unoriented system.

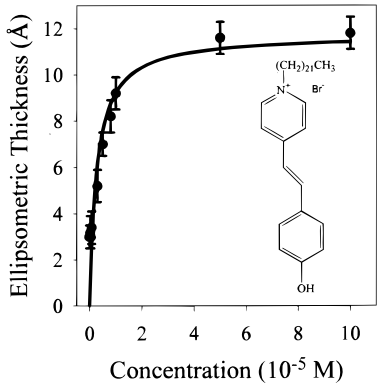

Figure 4. Adsorption isotherm for DPB films prepared by substrate dipping. The solid line is a Langmuir fit to the data, yielding a ΔG for adsorption of −3.2 kJ/mol. For an asymptotic monolayer film thickness of ∼12 Å and a molecular length for DPB of ∼35 Å, treating the DPB molecule as a rigid rod suggests an orientation angle of ∼70°.

$$\sin^2 \gamma^* = (2a_Z - a_X)/(2a_Z - a_X + a_Y) \qquad (14)$$

For an experimental geometry with hexanes flowing through the TIR cell and a fused-silica prism, orientation-independent absorbance is achieved for a polarization rotation angle of 54.73°. The fact that the calculated value of γ^* is nearly identical to the magic angle of 54.74° is coincidental, since γ^* will vary significantly with the refractive index of both the prism and the acoustic coupling liquid.

Case 1. Physisorbed Stilbene Dye Films. The adsorption isotherm for DPB stilbene dye films is shown in Figure 4, along with the chemical structure of the dye. Isotherm data were acquired by dipping substrates in varying concentrations of DPB in chloroform and recording the film thickness measured by ellipsometry. The film thickness reaches a maximum value of ∼12 Å for concentrations in excess of 10^{-4} M DPB, corresponding to completed monolayer formation. Assuming the DPB molecules may be treated as rigid, tightly packed, rodlike molecules 35 Å

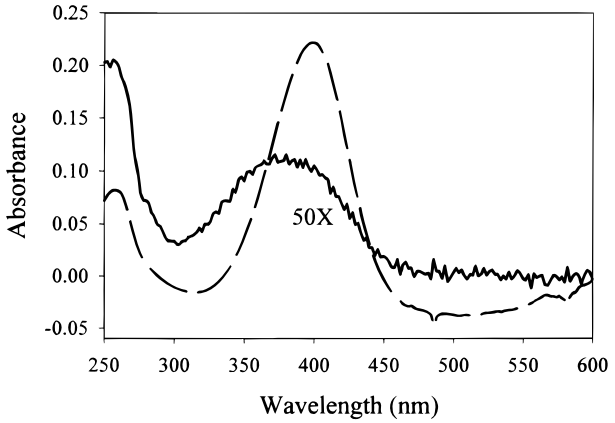

Figure 5. UV−visible absorbance spectra for DPB: monolayer film dipped in 8×10^{-4} M DPB (solid line), and 10^{-5} M DPB in chloroform (dashed line). The monolayer absorbance has been multiplied by 50 for comparative purposes.

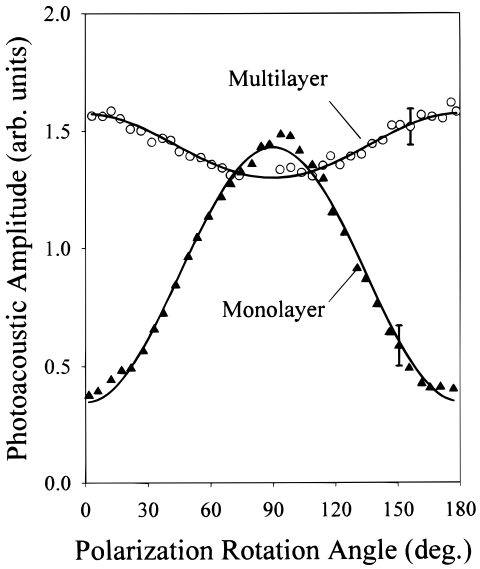

Figure 6. Averaged, normalized angle-resolved photoacoustic amplitudes acquired for both monolayer films of DPB (solid triangles, 16 measurements) and multilayer films consisting of a monolayer film with surface-aggregated DPB particulates (open circles, 16 measurements). The solid lines are fits to the data using eq 6b with the fitting coefficients given in Appendix III. A representative error bar ($\pm 1\sigma$) is provided on each curve.

in length, a film thickness of 12 Å corresponds to a geometric molecular tilt angle of ∼70°.

UV−visible absorbance spectra are shown in Figure 5 for DPB both on a quartz slide dipped in 8×10^{-5} M DPB and in a dilute chloroform solution (10^{-5} M). A noticeable blue-shift is observed in the absorbance spectrum of the surface-bound film (∼25 nm), most likely related to the change in environment in going from a nonpolar solvent to a polar surface. On the basis of the integrated absorbance of the DPB film (Figure 5) in combination with the ellipsometry results (Figure 4), dipping in $\sim 10^{-4}$ M DPB yields a surface coverage for the completed monolayer of $\sim 9 \times 10^{13}$ molecules/cm^2.

The transition dipole moment and hyperpolarizability for DPB were evaluated using ZINDO/S electronic structure calculations in Hyperchem. The transition moment excited at 355 nm lies parallel with the long molecular axis. Additionally, the 355 nm long-axis transition has both the largest oscillator strength and the lowest frequency, suggesting the hyperpolarizability at 1064 nm will be dominated by its influence. For a two-state model, the hyperpolarizability depends on the transition moment orientation and the change in permanent dipole between the ground and excited states (see Appendix II.), both of which are calculated to be parallel with the molecular z'-axis. Therefore, a dominant $\beta_{z'z'z'}$ hyperpolarizability tensor element is expected for 1064 nm fundamental excitation. On the basis of these modeling results, $K_{iZ} = K_{z'Z}$ as per the assumption made in eq 4, and $D_{z'Z} = \chi_{ZZZ}/(\chi_{ZZZ} + 2\chi_{ZXX})$ consistent with eq 12.

The angle-resolved absorbance for monolayer films of DPB acquired using the TIR cell is shown in the lower curve of Figure 6. Monolayer films were prepared by dipping the total internal reflection prism in 10^{-4} M DPB/$CHCl_3$. The TIR cell was subsequently filled and maintained with hexanes in order to facilitate acoustic coupling to the piezoelectric transducer. Although DPB is only marginally soluble in hexanes, gradual dissolution of the surface-bound DPB into the hexanes was observed. The loss rate was significantly less than the time required for data acquisition, and the loss did not result in a detectable change in molecular orientation over time. From the ARAPD measurements, the orientation parameter, $K_{z'Z}$, was found to be equal to 0.09 ± 0.04 (see Table 1). If a narrow orientation distribution is assumed, the apparent orientation angle as expressed in eq 8 is equal to 73 ± 3°. The apparent orientation angle of the chromophore obtained by ARAPD is remarkably close to the calculated ellipsometry result of ∼70°.

In an attempt to minimize signal losses due to DPB solvation in hexanes, separate ARAPD measurements were conducted using a saturated solution of DPB in hexanes as the acoustic coupling medium. However, the photoacoustic response did not stabilize unless the surface remained in contact with the flowing hexanes solution for at least 1 h. ARAPD results acquired after the signal stabilized are shown in the topmost curve in Figure 6. In this case, an orientation parameter of $K_{z'Z} = 0.36 \pm 0.01$ was obtained, significantly different from that obtained from the monolayer sample. If a narrow distribution is assumed, the corresponding mean orientation angle is 53.2° ± 0.9°. Visual inspection of the TIR prism surface after contact with the DPB-saturated hexanes indicated that surface agglomeration of DPB particulates had occurred. In this set of investigations, the ARAPD response measured after prolonged contact with DPB-saturated hexanes is dominated by a randomly oriented particulate overlayer (or multilayer). Note that the apparent orientation angle measured by ARAPD of the particulate DPB is within 1.5° of the expected magic angle response obtained for an unoriented system (cf. 53.2° with 54.7°). This latter finding confirms the expressions used to determine the electric field amplitudes at the interface yield results consistent with expectations.

Second harmonic intensities for the DPB monolayer samples are shown in Figure 7a, while those of DPB multilayers are shown in Figure 7b. From theoretical fits of the *s*-polarized curves (using the fitting coefficients described in Appendix III), the value of the experimental constant, *C*, was evaluated by setting χ_{XXZ} arbitrarily equal to unity and fitting the data to eq 10. The relative values of χ_{ZXX} and χ_{ZZZ}, normalized to χ_{XXZ}, were then obtained by fitting

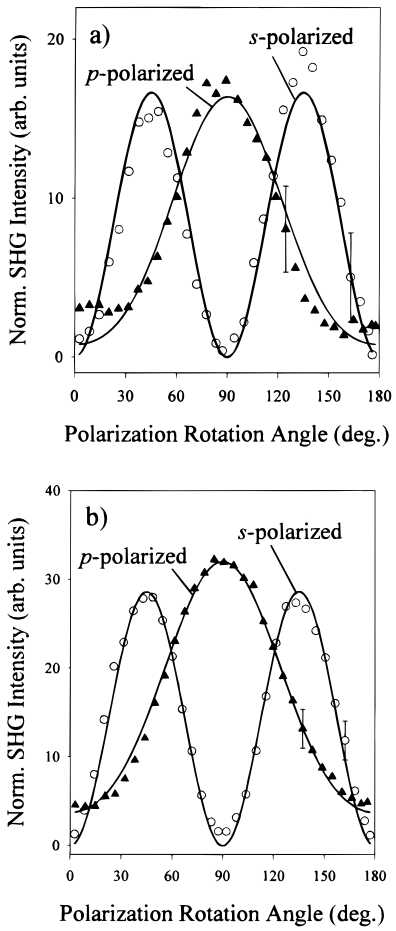

Figure 7. Averaged, normalized SHG results acquired for both monolayer films of DPB (a, four measurements) and multilayer films consisting of a monolayer film with surface-accumulated DPB (b, nine measurements). The solid lines are fits to the data using eqs 12 and 13 for the *s*-polarized (open circles) and *p*-polarized (solid triangles) second harmonics, respectively, with the fitting coefficients given in Appendix III. A representative error bar ($\pm 1\sigma$) is provided on each curve.

the *p*-polarized curve to eq 11 (or more precisely, eq AII.2) using the same constant, *C*. Because only the magnitude of χ_{XXZ} is retained from a fit of the *s*-polarized curve, the *p*-polarized data are fit equally well by χ_{XXZ} and χ_{ZXX} having both like and opposite signs, leading to two possible values for χ_{ZZZ}. Therefore, two sets of possible tensor elements are generated from a single measurement. Since χ_{XXZ} and χ_{ZXX} are expected to be of like sign and comparable magnitude for a dominant $\beta_{z'z'z'}$ (see Appendix II), orientation parameters and angles are reported only for the case of $\chi_{XXZ} = +1$. It is worth noting that the values of χ_{ZXX} normalized to χ_{XXZ} are within experimental error of unity for both mono- and multilayer DPB films (see Table 2). Equality between these two tensor elements is predicted theoretically for molecular systems dominated by a $\beta_{z'z'z'}$ hyperpolarizability tensor element (see eq AII.5). This relationship between the tensor elements supports two important aspects of the experiments; first, calculations indicating a dominant $\beta_{z'z'z'}$ for DPB appear to be reliable, and second, the expressions used to describe the both the fundamental and second harmonic electric fields at the interface are reasonably accurate. If either one of these experimental considerations was in fact inaccurate, a different ratio between the two tensor elements would likely result.

Table 1. ARAPD Results for the DPB and Azo Dye Films[a]

	DPB monolayer ($N = 16$)	DPB multilayer ($N = 16$)	azo dye ($N = 7$)
$K_{z'Z}$	0.09 ± 0.04	0.36 ± 0.01	0.27 ± 0.03
$\theta_{z'Z}$[b]	$73 \pm 3°$	$53.2 \pm 0.9°$	$58 \pm 2°$

[a] *N* equals the number of measurements made, errors are standard deviation. [b] Apparent orientation angle calculated by assuming a narrow orientation distribution.

In contrast to the ARAPD results, little difference is observed in the SHG response for the monolayer and multilayer films. Fits of the monolayer data yield an orientation parameter of $D_{z'Z} = 0.08 \pm 0.02$, indicating a mean orientation angle of $73 \pm 2°$ if a narrow distribution is assumed. For the multilayer data, the extracted orientation parameter is $D_{z'Z} = 0.11 \pm 0.03$, corresponding to an orientation angle of $70 \pm 3°$ for a narrow distribution. In both the monolayer and multilayer SHG orientation measurements, the narrow-distribution orientation angle is within error of the experimental ARAPD result, and again very close to the orientation angle predicted by the geometric film thickness.

The striking contrast in the behavior of the ARAPD and SHG data for the monolayer and multilayer regimes is an excellent example of the unique information available from a combination of nonlinear and linear spectroscopic techniques. ARAPD measurements are sensitive to absorbance from all DPB within the penetration depth of the evanescent field. Consequently, for particulates that adsorb to the surface (over the oriented monolayer), the signal response is dominated by the particulates rather than the monolayer film. In contrast, SHG arises only from noncentrosymmetrically oriented molecules. Adsorption of centrosymmetric, randomly oriented DPB particulates does not lead to coherent surface SHG, and the SHG response is still dominated by the nonlinear properties of the oriented surface layer. Therefore, while the ARAPD results are greatly influenced by the presence of the DPB particulates, no significant change is observed in the molecular orientation measured by SHG. A combination of absorbance and fluorescence would have yielded the unoriented response, with no surface specific information.

Case 2. Covalently Bound Azo Dye Films. Covalent attachment of the azo dye (see Figure 9) to the fused-silica surface was confirmed by water contact angle, ellipsometry, and UV−visible spectroscopy measurements. Upon reaction, the water contact angle changed from a value below detection (complete surface wetting) to a value of $60 \pm 5°$, indicating a significant alteration in surface hydrophobicity. Ellipsometry measurements at each step of the reaction indicate a film thickness of 5.0 ± 0.9 Å after the first reaction step with the monofunctional aminosilane and 6.2 ± 0.8 Å after surface attachment of the azo dye. Based on the 1.2 Å increase in film thickness, and an estimated length for the dye of 14 Å, the ellipsometry results suggest a surface coverage of ~9% of a monolayer. Surface coverage can also be estimated from the UV−visible absorbance of the surface film prepared on a quartz window. Using the azo dye molar absorptivity and the measured film absorbance (shown in Figure 8), the surface coverage of the dye was estimated to be 2.2×10^{13} mlcls/cm^2,

Table 2. SHG Results for the DPB and Azo Dye Films[a]

	DPB monolayer ($N = 4$)		DPB multilayer ($N = 9$)		azo dye ($N = 6$)	
χ_{XXZ}	1	−1	1	−1	1	−1
χ_{ZXX}	0.98 ± 0.08	0.98 ± 0.08	1.05 ± 0.09	1.05 ± 0.09	1.1 ± 0.2	1.1 ± 0.2
χ_{ZZZ}	0.16 ± 0.12	0.3 ± 0.1	0.31 ± 0.06	0.40 ± 0.06	1.9 ± 0.4	2.39 ± 0.4
$D_{z'Z}$	0.08 ± 0.02		0.11 ± 0.03		0.48 ± 0.03	
$\theta_{z'Z}$[b]	73 ± 2°		70 ± 3°		46 ± 2°	

[a] N equals the number of measurements made, errors are standard deviation. [b] Apparent orientation angle calculated by assuming a narrow orientation distribution.

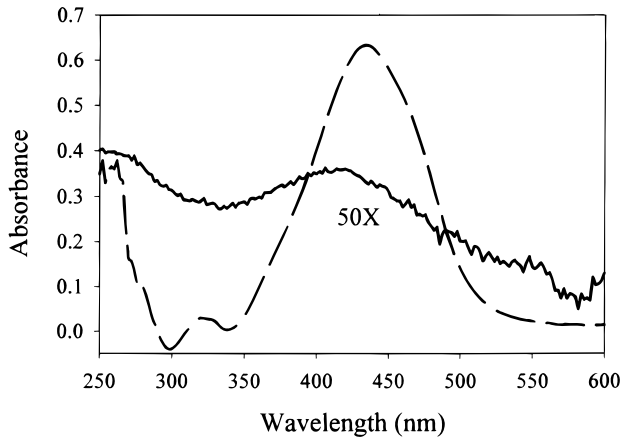

Figure 8. UV−visible absorbance spectra for the azo dye: submonolayer film prepared by surface reaction (solid line) and an 8 × 10^{-4} M solution in toluene (dashed line). The monolayer absorbance has been multiplied by 50 for comparative purposes.

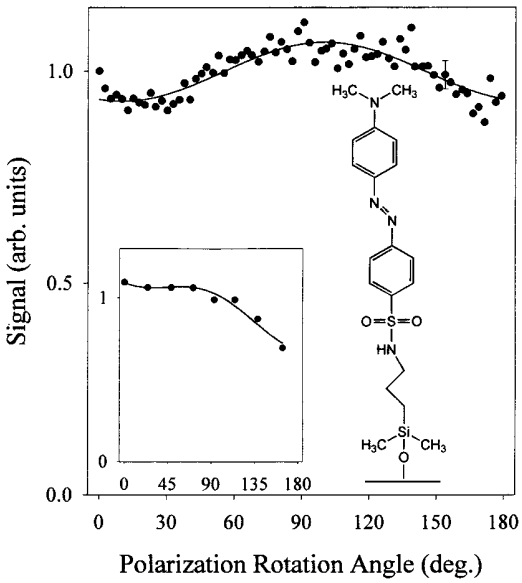

Figure 9. Corrected, averaged ARAPD results acquired for the surface-bound azo dye (chemical structure shown in the figure, seven measurements). During ARAPD data acquisition, the signal was observed to decay significantly over time (representative raw data are shown in the inset plot). Orientation measurements were made using the raw ARAPD data, fit to a function incorporating both an exponential decay to a constant and the polarization dependent absorbance (shown by the solid line in the inset plot). In the main figure itself, averaged, normalized data are shown for comparative purposes after correcting for only the time-dependent signal loss. The solid line is a fit to the corrected data using eq 6b with the fitting coefficients given in Appendix III. A representative error bar (±1σ) is provided on the upper curve.

which corresponds to ∼8% of a monolayer assuming an approximate molecular area of 37 Å^2. From both the ellipsometry and absorbance measurements, it may be concluded that the reaction procedure generates submonolayer coverages (∼$^1/_{10}$ of a monolayer) of the azo dye.

ARAPD results for the covalently bound azo dye chromophore are shown in Figure 9 and summarized in Table 1. SHG curves for the same system are shown in Figure 10. During ARAPD data acquisition, the signal was observed to decay significantly over time (representative raw data are shown in the inset plot of Figure 9). Experimental evidence implicates cleavage of the N−S bond as the likely photochemical loss mechanism. Orientation values were obtained from the raw ARAPD data by fitting to a function incorporating an exponential decay to a constant as well as the polarization dependent absorbance described in eq 6. No signal loss was observed over time during SHG data acquisition, as no light was absorbed by the azo dye molecules.

Molecular modeling calculations indicate that, similar to the DPB stilbene dye, both the transition moment of the azo dye excited at 355 nm and the dominant hyperpolarizability tensor element ($\beta_{z'z'z'}$) for a 1064 nm fundamental wavelength are directed parallel with the long molecular axis. Accordingly, the molecular orientation of the azo dye can be evaluated using the same relations as used for DPB [i.e., $K_{fZ} = K_{z'Z}$ and $D_{z'Z} = \chi_{ZZZ}/(\chi_{ZZZ} + 2\chi_{ZXX})$]. As with DPB, a dominant $\beta_{z'z'z'}$ is supported by an experimental ratio of χ_{ZXX}/χ_{XXZ} within error of unity (see Table 2). ARAPD measurements of the azo dye long-axis orientation yield an orientation parameter of $K_{z'Z} = 0.27 \pm 0.03$ or an apparent molecular tilt angle of 59 ± 2° if a narrow distribution is assumed. SHG measurements yield an orientation parameter of $D_{z'Z} = 0.48 \pm 0.03$, corresponding to an apparent tilt angle of 46 ± 2°. The inconsistency in apparent molecular tilt angles implies that the assumption of a narrow angular distribution is not valid.

Combining SHG and ARAPD Results. If the assumption of a narrow molecular orientation distribution is relaxed and a Gaussian distribution is assumed,[6−10] a single measurement is no longer sufficient to determine both the mean and the width of the angular distribution. This ambiguity can be removed by combining both ARAPD and SHG measurements of the same molecular system. As shown in Figure 11, for a Gaussian distribution there is range of possible solutions satisfying a single measurement, with one extreme being an infinitely narrow distribution and the other a potentially broad distribution. The point at which the ARAPD and SHG curves cross indicates the distribution width and mean which are consistent with both measured orientation parameters (shown in Figure 11a for DPB

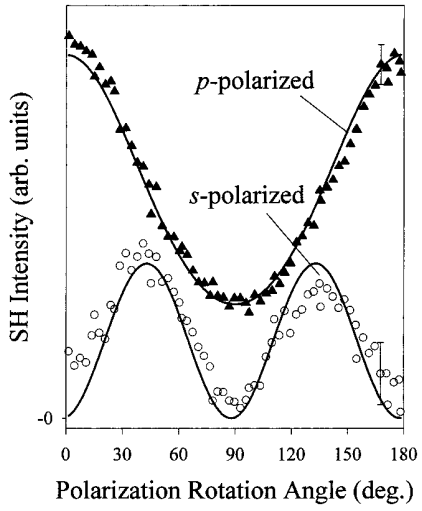

Figure 10. Averaged, normalized SHG results acquired for films of the azo dye (six measurements). The solid lines are fits to the data using eqs 12 and 13 for the *s*-polarized (open circles) and *p*-polarized (solid triangles) second harmonics, respectively, with the fitting coefficients given in Appendix III. A representative error bar ($\pm 1\sigma$) is provided on each curve.

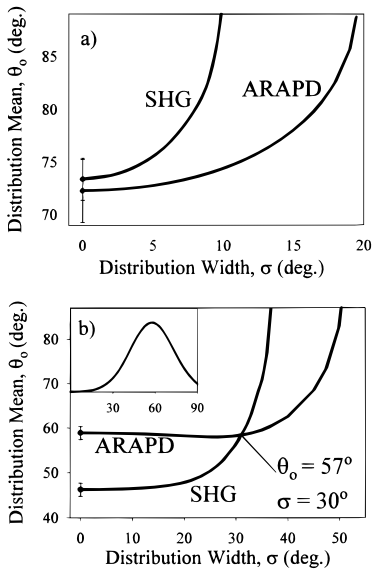

Figure 11. SHG and ARAPD molecular orientation measurements combined to yield both the means (θ_o) and rms widths (σ) of the orientation distributions for DPB (a) and the azo dye (b). Each curve indicates the range of Gaussian distributions which can yield the experimental orientation parameter obtained by either the SHG or ARAPD orientation measurement alone. The point at which the ARAPD and SHG curves cross represents the distribution mean and width, which is consistent with both measurements. For DPB, the two curves are within error in the limit of a narrow distribution, while for the azo dye the distribution mean is 57° and the width is 30°. The corresponding orientation distribution for the azo dye is shown in the inset plot in (b) for angles from 0 to 90°.

and Figure 11b for the azo dye). This crossover point is the graphical equivalent of solving two equations with two unknowns. For DPB films, the two spectroscopic measurements yield almost identical orientation parameters, within experimental error of each other in the limit of a narrow orientation distribution. Based on the magnitudes of the experimental errors, it may be concluded that the orientation distribution for the DPB monolayers is centered around 73° with a distribution width of less than ~8° (i.e., the width at which the experimental errors no longer overlap). In contrast, the azo dye yields a Gaussian distribution mean of 57° with a root-mean-square (rms) width of 30°. The distribution is shown the inset of Figure 11b. Although the assumption of a narrow distribution has been proven accurate for the case of DPB, it fails to reliably describe the orientation distribution for the azo dye.

A possible explanation for the significant difference in distribution widths for DPB and the azo dye system may be proposed by considering the likely orienting interactions in the two cases. For the azo dye films, dye molecules are covalently attached at specific locations for a surface coverage of less than $^1/_{10}$ of a monolayer, suggesting that the predominant orienting interactions are those of the isolated chromophore. By inspection of the surface-bound structure of the azo dye, free rotation about the propyl chain near the base of the chromophore may allow for a wide range of motion of the chromophore itself. It is reasonable to propose that this wide range of motion leads to a broad range of accessible chromophore orientations for the azo dye. In contrast, the dominating orienting forces for the DPB surface films are most likely a combination of intermolecular interactions between the chromophores and interactions between the long aliphatic hydrocarbon chains. Assembly of neighboring molecules into highly ordered structures would naturally lead to a high degree of chromophore order as well, and a corresponding narrow orientation distribution.

On the basis of the azo dye and DPB results, it is tempting to suggest general guidelines for cases in which the assumption of a narrow distribution is expected to be reasonable and cases in which it will most likely fail. For molecular surface systems in which the orientation is dominated by intermolecular interactions to form ordered assemblies, including long-chain trifunctional silane self-assembled monolayers and tightly packed Langmuir and Langmuir−Blodgett films, the distribution in orientation angles in the fully assembled monolayer film may be reasonably assumed to be narrow. In contrast, the assumption of a narrow distribution may be quite poor for monolayer systems in which orientation is dominated by local interactions, particularly if a range of orientations is accessible through intramolecular reorientation.

In summary, SHG and ARAPD measurements were combined to measure molecular orientation in a total internal reflection flow cell. From a single measurement, an infinite number of possible orientation distributions could be generated to satisfy the individual orientation parameters, ranging from narrow distributions to fairly broad distributions. However, by combining the two linearly independent measurements, both the mean orientation angle and the angular distribution can be evaluated. Two molecular systems were investigated, one of which was demonstrated to possess a narrow orientation distribution (rms width of less than ~8°) and another a fairly broad distribution (rms width of 30°). Differences in the structure of the surface films were proposed to account for the significant difference in the angular distributions of the two systems.

ACKNOWLEDGMENT

The authors gratefully acknowledge support from the National Science Foundation.

APPENDIX I. PHOTOACOUSTIC RESPONSE FROM AN INTERFACIAL FILM

For a laser beam radius (R_s) much larger than the product of the speed of sound through the medium of interest (v) and the laser pulse width (τ_L), the area of excitation may be assumed to be πR_s^2 (for quartz and organic solvents with a pulse width of 10 ns, $v\tau_L$ values will range from ~0.01 to 0.06 mm, for a beam radius of ~0.5 cm). Since the thickness of the surface film (a few angstroms) will be significantly less than $v\tau_L$, the depth (d) of the source volume (V) may be assumed to be $v\tau_L$, and the volume to be $\pi R_s^2 v\tau_L$.[22,23] As the source volume is essentially a flat disk, the acoustic wave generated may be assumed to be formed via a pistonlike expansion in thickness, with a negligible contribution arising from the increase in circumference. Consequently, the change in source volume, ΔV, may be approximated by eq AI.1[22,23]

$$\Delta V = \beta V \Delta T = \pi R_s^2 \, \Delta d \tag{AI.1}$$

where β is the expansion coefficient of the medium, ΔT is the change in source temperature resulting from absorption, and Δd is the change in thickness of the acoustic source.

At the interface between two media, heat deposition into both media can occur. If it is assumed that the change in temperature upon excitation is identical across the interface (i.e., $\Delta T_1 = \Delta T_2 = \Delta T$, where the subscripts indicate the medium), then the energy absorbed at the interface (E_{abs}) will be distributed to both volume elements. This treatment is similar to descriptions of photoacoustics at surfaces in contact with air.[30] The change in interfacial temperature upon light absorption is given by

$$\Delta T = E_{abs}/(\rho_1 V_1 C_{p1} + \rho_2 V_2 C_{p2}) \tag{AI.2}$$

where ρ_i is the density of medium i, V_i is the volume element of medium i into which the heat is deposited, and C_{pi} is the heat capacity of medium i.

For an optically thin surface film, the energy absorbed (E_{abs}) is equal to the incident energy (E_0) multiplied by the absorption cross section (σ_{abs}) and the surface coverage (θ). For an oriented system, the absorption cross section will be a function of both the incident wavelength and the incident polarization.

$$E_{abs} = E_0 \theta \sigma_{abs} \tag{AI.3}$$

Neglecting losses in the acoustic displacement associated with damping and geometric expansion, the peak acoustic pressure in medium i, P_i, measured at the piezoelectric detector is given by eq AI.4. The neglect of damping can be justified for our experimental setup, since the concomitant reduction in amplitude is included in an instrumental response constant.[22,23]

$$P_1 = c_1 \rho_1 \Delta d_1 / \tau_L \tag{AI.4}$$

Combining eqs AI.1−AI.4 yields the following relationship between the photoacoutic amplitude (proportional to the signal, S) and the experimental variables:

$$S \propto P_1 = \frac{E_0 \theta \sigma_{abs} \tau_L \beta_1}{\rho_1 \pi R_s^2 (c_1 \rho_1 C_{p1} + c_2 \rho_2 C_{p2})} \tag{AI.5}$$

Despite the number of approximations in the proposed model, it successfully predicts the most salient features of the photoacoustics experiments; namely, that the amplitude of the detected signal is directly proportional to the incident beam energy, sample absorbance cross section, and sample coverage (for a constant absorption cross section). Previous studies of Rose Bengal have confirmed the linear dependence of the photoacoustic amplitude on both the incident beam energy and the sample number density.[20]

APPENDIX II. THEORY AND TREATMENT OF THE SHG MEASUREMENTS

The following discussion of SHG is presented with the intention of providing all the detail necessary for the reader to understand how the data were treated. While many of the expressions may be readily found in the literature, the complete treatment is much less available.

Fitting Procedure. Data were fit according to the relation in eqs 10 and 11. In a total internal reflection geometry, the SHG fitting coefficients will have both real and imaginary components.[28] If the $\chi^{(2)}$ tensor elements are assumed to be predominantly real (a reasonable assumption far from resonance), the data can be fit by the following expressions:

$$I_s = C \sin^2(2\gamma) \chi_{XXZ}^2 |s_1|^2 \tag{AII.1}$$

$$I_p = C \cdot \mathrm{Re}\{[s_5\chi_{ZXX} + \cos^2\gamma(s_2\chi_{XXZ} + s_3\chi_{ZXX} + s_4\chi_{ZZZ} - s_5\chi_{ZXX})]^2\} + C \cdot \mathrm{Im}\{[s_5\chi_{ZXX} + \cos^2\gamma(s_2\chi_{XXZ} + s_3\chi_{ZXX} + s_4\chi_{ZZZ} - s_5\chi_{ZXX})]^2\} \tag{AII.2}$$

where C is an experimental constant incorporating both the constant terms in eq AII.2 and the instrument response function. If the constant, C, is known, then measurements of the s- and p-polarized second harmonic intensities for different fundamental polarization rotation angles will yield the magnitudes of the individual three independent tensor elements. If C is not known, fits of the data to eqs AII.1 and AII.2 will yield relative values of the tensor elements. In our experiments, only relative values of the tensor elements were measured.

Orientation from the Molecular Hyperpolarizability. The individual surface second-order nonlinear polarizability tensor elements are related to the molecular second-order nonlinear polarizability, $\beta^{(2)}$, by ensemble averages over molecular orientation:[27]

$$\chi_{ijk} = N_s \sum_{\lambda\mu\nu} \langle \mathbf{T}_{ijk}^{\lambda\mu\nu} \rangle \beta_{\lambda\mu\nu} \tag{AII.3}$$

(30) Rosencwaig, A. *Photoacoustics and Photoacoustic Spectroscopy*; John Wiley and Sons: New York, 1980; Chapters 9, 10.

where N_s is the surface density of molecules, **T** is a transformation matrix defining the angular relations between the molecular coordinate system (λ,μ,ν) and the surface coordinate system (i,j,k), and the brackets indicate an ensemble average. If $\beta^{(2)}$ is known and measurements are made to characterize $\chi^{(2)}$, information regarding molecular orientation can be determined. For nonresonant SHG measurements with an orientation distribution which is isotropic within the surface plane, the three nonzero, independent tensor elements are given by[27]

$$\chi_{ZZZ} = N_s[\langle\cos^3\theta_{z'Z}\rangle\beta_{z'z'z'} + \langle\cos\theta_{z'Z}\sin^2\theta_{z'Z}\sin^2\Psi\rangle(\beta_{z'x'x'} + 2\beta_{x'x'z'})] \quad \text{(AII.4a)}$$

$$\chi_{ZXX} = \frac{1}{2}N_s\begin{bmatrix}\langle\cos\theta_{z'Z}\sin^2\theta_{z'Z}\rangle\beta_{z'x'x'} + \langle\cos\theta_{z'Z}\rangle\beta_{z'x'x'} \\ -\langle\cos\theta_{z'Z}\sin^2\theta_{z'Z}\sin^2\Psi\rangle(\beta_{z'x'x'} + 2\beta_{x'x'z'})\end{bmatrix} \quad \text{(AII.4b)}$$

$$\chi_{XXZ} = \chi_{XZX} = \frac{1}{2}N_s\begin{bmatrix}\langle\cos\theta_{z'Z}\sin^2\theta_{z'Z}\rangle\beta_{z'z'z'} + \langle\cos\theta_{z'Z}\rangle\beta_{x'x'z'} \\ -\langle\cos\theta_{z'Z}\sin^2\theta_{z'Z}\sin^2\Psi\rangle(\beta_{z'x'x'} + 2\beta_{x'x'z'})\end{bmatrix} \quad \text{(AII.4c)}$$

where Ψ is the Euler rotation angle about the molecular z'-axis. Since the X- and Y-axes in the surface plane are equivalent, $\chi_{YYZ} = \chi_{YZY} = \chi_{XXZ}$ and $\chi_{ZYY} = \chi_{ZXX}$.

For rodlike molecules with a single dominant component of the molecular hyperpolarizability tensor directed along the long molecular axis (i.e., $\beta_{z'z'z'}$ is dominant), the surface hyperpolarizability tensor elements given by eq AII.4 simplify to

$$\chi_{ZZZ} = N_s\langle\cos^3\theta_{z'Z}\rangle\beta_{z'z'z'} \quad \text{(AII.5a)}$$

$$\chi_{ZXX} = \chi_{XXZ} = \frac{1}{2}N_s\langle\cos\theta_{z'Z}\sin^2\theta_{z'Z}\rangle\beta_{z'z'z'} \quad \text{(AII.5b)}$$

From these relations, the expression reported in eq 12 is easily derived.

Calculation of the Molecular Hyperpolarizability. For a simple two-state system (i.e., ground and excited states) the relative magnitudes of the individual components of the molecular hyperpolarizability tensor, $\beta^{(2)}$, may be evaluated using eq AII.6,[26,31]

$$\beta_{\lambda\mu\nu}(\omega) = \frac{-e^3}{2\hbar^2(\omega_{ng}{}^2 - \omega^2)}\left[\Delta d^{\lambda}_{ng}\, r^{\mu}_{ng}\, r^{\nu}_{ng} + r^{\lambda}_{ng}(r^{\mu}_{ng}\,\Delta d^{\nu}_{ng} + \Delta d^{\mu}_{ng}\, r^{\nu}_{ng})\frac{\omega_{ng}{}^2 + 2\omega^2}{\omega_{ng}{}^2 - (2\omega)^2}\right] \quad \text{(AII.6)}$$

in which ω is the optical frequency of the fundamental beam, $\hbar\omega_{ng}$ is the energy difference between the ground state (g) and the excited state (n), Δd^{i}_{ng} is the change in permanent dipole from the ground to excited state projected along the molecular i-axis, r^{i}_{ng} is the transition dipole moment projected along the molecular i-axis, and ω is the fundamental optical frequency. Resonance enhancement occurs both when $\omega = \omega_{ng}$, and when $\omega = {}^1/_2\omega_{ng}$ (i.e., when the fundamental or second harmonic is resonant with a real state). It is worth noting that eq AII.6 is only valid for optical frequencies far from resonance, where the molecular hyperpolarizability is purely real.

Molecular modeling calculations can be performed to evaluate the orientations of relevant transition moments, as well as the difference in permanent dipole between the ground and excited states. With these parameters, relative magnitudes of the individual tensor elements may be calculated. More general forms of the expression in eq AII.6 including contributions from multiple transitions[31] and for resonance-enhanced SHG investigations[32−34] can be used in instances where use of eq AII.6 is not justified.

APPENDIX III. FRESNEL FACTORS FOR ARAPD AND SHG IN THE TIR CELL

For the TIR cell employed in this study, the fitting coefficients introduced in eq 6 are derived by projection onto the interfacial coordinates:

$$a_X = |\cos\theta_I^{\omega}\, L_{XX}^{\omega}|^2 \quad \text{(AIII.1a)}$$

$$a_Y = |L_{YY}^{\omega}|^2 \quad \text{(AIII.1b)}$$

$$a_Z = |\sin\theta_I^{\omega}\, L_{ZZ}^{\omega}|^2 \quad \text{(AIII.1c)}$$

in which θ_I^{ω} is the internal angle of incidence with respect to the total internal reflection surface for a given frequency of light, and each L_{ii}^{ω} term is a Fresnel factor describing the interfacial electric field amplitude for the component of light directed along the i-axis. Expressions for the Fresnel factors employed in these investigations are given below.

$$L_{XX}^{\omega} = t_{p12}^{\omega}(1 - r_{p23}^{\omega}) \quad \text{(AIII.2a)}$$

$$L_{YY}^{\omega} = t_{s12}^{\omega}(1 + r_{s23}^{\omega}) \quad \text{(AIII.2b)}$$

$$L_{ZZ}^{\omega} = t_{p12}^{\omega}(1 + r_{p23}^{\omega})\frac{1}{2}[1 + (n_2^{\omega}/n_3^{\omega})^2] \quad \text{(AIII.2c)}$$

where t_{ij}^{ω} and r_{ij}^{ω} are transmission and reflection coefficients at the ij interface for a given frequency, ω, with subscripts s and p indicating s- and p-polarized light, and n_i is the refractive index of medium i, where medium 1 is air, medium 2 is the fused-silica prism, and medium 3 is the solvent in the flow cell (explicit expressions for the reflection and transmission coefficients can be found in ref 35). The transmission coefficients with subscripts "12" account for reflective losses at the entrance interface, while the reflection coefficients with subscripts "23" describe reflection

(31) Oudar, J. L.; Zyss, J. *Phys. Rev. A* **1983**, *26*, 2016−2027.

(32) Higgins, D. A.; Byerly, S. K.; Abrams, M. B.; Corn, R. M. *J. Phys. Chem.* **1991**, *95*, 6984−6990.

(33) Higgins, D. A.; Byerly, S. K.; Abrams, M. B.; Corn, R. M. *Langmuir* **1992**, *8*, 1994−2000.

(34) Ward, J. F. *Rev. Mod. Phys.* **1965**, *37*, 1−18.

(35) Jenkins, F. A.; White, H. E. *Fundamentals of Optics*; McGraw-Hill: New York, 1957; pp 529−532.

at the TIR interface. For total internal reflection, the reflection coefficients are complex.[36]

The Fresnel factors in eq AIII.2 follow from standard expressions for the electric fields at an interface.[35,36] The electric field amplitude at a bare interface consists of two contributions, one from the incident field and one from the reflected field, which may interfere either constructively or destructively. In contrast to the *X*- and *Y*- polarized components, the *Z*-polarized electric field amplitude is discontinuous across the interface, changing by a factor of $(n_2/n_3)^2$ from its value in the prism to its value in the solvent. Rather than assuming the monolayer can be treated as being located in either the incident or refractive medium, the average electric field of the two media was used (as can be seen in eq AIII.1c). The sensitivity of the calculated orientation angles on the *Z*-component of the interfacial electric field was tested by fitting the ARAPD data, assuming electric field amplitudes representative of both the silica and the solvent. In all cases, the different treatments yielded differences in orientation angles of less than a few degrees from the reported values. For SHG the fitting coefficients described in eqs 10 and 11 are given to be[28,37]

$$s_1 \equiv L_{yy}^{2\omega}\, L_{yy}^{\omega}\, L_{zz}^{\omega} \sin \theta_{\mathrm{I}}^{\omega} \qquad \text{(AIII.3a)}$$

$$s_2 \equiv L_{xx}^{2\omega}\, L_{xx}^{\omega}\, L_{zz}^{\omega} \sin(2\theta_{\mathrm{I}}^{\omega}) \cos \theta_{\mathrm{R}}^{2\omega} \qquad \text{(AIII.3b)}$$

$$s_3 \equiv L_{zz}^{2\omega}(L_{xx}^{\omega})^2 \cos^2 \theta_{\mathrm{I}}^{\omega} \sin \theta_{\mathrm{R}}^{2\omega} \qquad \text{(AIII.3c)}$$

$$s_4 \equiv L_{zz}^{2\omega}(L_{zz}^{\omega})^2 \sin^2 \theta_{\mathrm{I}}^{\omega} \sin \theta_{\mathrm{R}}^{2\omega} \qquad \text{(AIII.3d)}$$

$$s_5 \equiv L_{zz}^{2\omega}(L_{yy}^{\omega}) \sin \theta_{\mathrm{R}}^{2\omega} \qquad \text{(AIII.3e)}$$

where L_{ii}^{ω} are the linear Fresnel coefficients previously employed in describing the electric fields for ARAPD investigations, $L_{ii}^{2\omega}$ are nonlinear Fresnel factors describing the detected electric field amplitudes of the second harmonic per unit amplitude generated at the interface, and $\theta_{\mathrm{R}}^{2\omega}$ is the reflection angle of the second harmonic (neglecting dispersion, $\theta_{\mathrm{R}}^{2\omega}$ and $\theta_{\mathrm{I}}^{\omega}$ are equal).

The linear Fresnel factors for SHG have exactly the same form as those used for ARAPD in eq AIII.2, with the exception that the reflection and transmission coefficients are all evaluated for a wavelength of 1064 nm. The nonlinear Fresnel factors are given by

$$L_{xx}^{2\omega} = -(1 - r_{p23}^{2\omega})t_{p21}^{2\omega} \qquad \text{(AIII.4a)}$$

$$L_{yy}^{2\omega} = (1 + r_{s23}^{2\omega})t_{s21}^{2\omega} \qquad \text{(AIII.4b)}$$

$$L_{ZZ}^{2\omega} = (1 + r_{p23}^{2\omega})\frac{1}{2}[1 + (n_2^{2\omega}/n_3^{2\omega})^2]t_{p21}^{2\omega} \qquad \text{(AIII.4c)}$$

The fundamental basis of the expressions in eq AIII.4 is analogous to that used to generate the linear Fresnel factors, described earlier.

Received for review November 10, 1999. Accepted January 3, 2000.

AC9912956

(36) Harrick. N. J. *Internal Reflection Spectroscopy*; Interscience Publishers: New York, 1967; Chapter 2.

(37) Naujok, R. R.; Higgins, D. A.; Hanken, D. G.; Corn, R. M. *J. Chem. Soc., Faraday Trans.* **1995**, *91*, 1411−1420.